This is a repository copy of *A Monte Carlo simulator to investigate cell-to-cell deviation in a grid-tied battery pack*.

White Rose Research Online URL for this paper:
https://eprints.whiterose.ac.uk/185510/

Version: Published Version

IET Power Electronics

The Institution of Engineering and Technology   WILEY

ORIGINAL RESEARCH

A Monte Carlo simulator to investigate cell-to-cell deviation in a grid-tied battery pack

Zeyuan Wang (ID) | **Zhuo Wang** | **Jonathan Davidson** (ID) | **Martin Foster** | **Daniel Gladwin**

Department of Electronic and Electrical Engineering, The University of Sheffield, Sheffield, UK

Correspondence
Jonathan Davidson, Department of Electronic and Electrical Engineering, The University of Sheffield, Sir Frederick Mappin Building, Sheffield, S1 3JD, UK.
Email: jonathan.davidson@sheffield.ac.uk

Abstract

Battery energy storage systems (BESSs) are commonly used in smart grids. Voltage deviation or imbalance among cells generally exists in multi-cell battery packs. This work presents a study of the voltage deviation-related phenomena observed during the operation of a grid-tied BESS, Willenhall Energy Storage System (WESS), including the voltage deviation changes during full range cycle and the cut-off mechanism activated by it. Electroimpedance spectroscopy measurements and equivalent circuit modelling were conducted on the same type of cell as that used in WESS to obtain cell-equivalent circuit parameter distributions (the standard deviation and mean). Cell voltage deviation in a WESS-sized battery pack (> 21k cells) was studied using Monte Carlo simulation through a proposed cell level battery simulator. Both experiments and simulations reveal that high cell voltage deviation emerges at the low and high state-of-charge zones where the cell internal resistance has a large value and large extent of deviation.

1 | INTRODUCTION

As renewable energy penetrates electricity grids, traditional grids are evolving into smart grids where energy storage is used to provide rapid grid services. In the UK, renewable energy represents a significant part of generated electricity. Taking the first quarter of 2021 as an example, renewable energy contributed 41.6% of the electricity in the UK [1]. Renewable energy such as solar PV and wind power can be easily influenced by weather conditions which reduce the reliability of the grid. As a key component in smart grids, battery energy storage systems (BESS) can compensate for this side effect of renewable energy [2] and help maintain a stable utility frequency. Normally, lithium-ion batteries are preferred in a smart grid because they have high power and energy capacities and low self-discharge [3].

The battery pack in a smart grid normally consists of a large number of cells where all cells are constrained to operate inside a certain voltage range by the battery management system (BMS) to prevent cell damage from undesired physical and chemical changes such as collector dissolution and lithium dendrites [4]. There is variation in manufacturing tolerance,

impurities etc, which eventually leads to differences between cells, which can be observed in the terminal voltage. In the battery packs without active balancing, the overall pack performance is limited by the 'worst' cell [5], which reduces the energy utility of other cells. Inside a grid-tied BESS, without active balancing this energy loss becomes considerable due to its scale.

Cell-to-cell variation (CtCV) is generally classified by whether it is brought about by intrinsic or extrinsic sources [6, 7]. The intrinsic variations are caused by the difference in cell chemistry and electrical properties: for example, the impedance and capacity. On the other hand, factors like the unevenness of ambient temperature, cooling system and external circuits are considered extrinsic sources. These variation sources also influence each other in difficult-to-predict ways [8].

Experiments and statistical analysis on CtCV have been widely conducted on cells with different sample sizes, from dozens [9] to hundreds [10] and even thousands [11, 12]. Studied sources of CtCV normally include operating temperature, capacity, weight, DC resistance, AC impedances, self-discharge and calendar ageing. Measurements with larger sample sizes (such as [11, 12]) are generally more reliable.

The experimental results provide statistical data for variation research based on a simple electrical model [13]. In more sophisticated electrochemical models [14, 15], the variation sources are considered from other quantities such as the electrode thickness, electrode density and weight fraction of active material.

Because of CtCV sources like internal resistance, the current and heat generation (hence temperature) among cells can be slightly different in an operating battery. Cell ageing is a slow process dependent on current and temperature [16] so that, after a long time, cells in a pack will age unevenly and eventually significantly influence the battery pack performance. In the study of these ageing-related long-term effects, the relatively small battery time constants are normally ignored in both measurement and simulation and the cell variation is considered to be state-of-charge (SoC)-independent. However, the low fidelity of empirical ageing models makes it less credible to distinguish the ageing difference among cells caused by the small CtCV and omitting the impact of SoC on CtCV could lead to inaccurate battery modelling.

With the development of new battery manufacturing and material technologies, the lifetime of some cells such as lithium titanate oxide (LTO) has exceeded several thousand cycles [17] which indicates a slow ageing process. Meanwhile, good short-term dynamic battery performance becomes more important in certain applications such as grid-support services [18] and the buffering of regenerated energy in railways [19, 20]. The improvement in battery lifetime and the aforementioned special demand in emerging applications make the study of the effects of CtCV on battery performance in short-term (time-limited) events meaningful.

Under the control of the BMS, a battery pack is normally operated under certain restrictions including the limitations of temperature, continuous and peak current value for charging and discharging, and operating voltage. These limitations define a cell's operating area known as 'safety operating zone' [21]. A BMS has some flexibility in restricting a battery inside the allowed voltage range by managing battery SoC and current. The energy management system also must avoid operating the battery at nearly charged or discharged states so that the battery's open-circuit voltage (V_{OC}), and hence terminal voltage, are away from (and between) the maximum and minimum allowed voltage. Additionally, the energy management system would adjust the battery current to keep the battery terminal voltage within the safety zone.

Equivalent circuit models (ECMs) are commonly used in battery simulation which uses electrical components such as resistors, capacitors and voltage sources to represent battery's ohmic resistance, diffusion process and V_{OC} respectively [22]. In some cases, the values of these lumped parameters change dynamically with V_{OC}, SoC and state of health. Different cells can be represented by the same ECM with different electrical component values. For the cells from the same factory and batch, their ECM electrical component values usually follow a statistical distribution which can be identified by sampling experiments. With knowledge of the ECM electrical component value distributions, cell parameters for modelling can be randomly generated.

An ECM for a multi-cell battery pack considering CtCV can then be constructed by connecting these individual cell ECMs.

The study of CtCV is not only important for the BMS design but also for improving battery performance and architecture. Inside a battery pack, cell terminal-voltage deviation is a consequence of CtCV. After long operation, the battery pack performance can be damaged by CtCV. Reference [23] indicates that an initial CtCV accelerates the battery ageing, while [24] shows that battery-pack ageing can be reduced by active voltage balancing. Apart from improving battery pack ageing performance, the study of CtCV also benefits the battery module architecture design [25]. Insufficient management of CtCV could lead to catastrophic failure of a BESS. For example, on 19 April 2019, an explosion occurred due to a single-cell failure in a 2 MW/2 MWh BESS near Phoenix, USA, when the battery was charged to 90% SoC [26, 27]. With the increasing awareness of the importance of CtCV, modern battery pack techniques (e.g. cell balancing [28], manufacturing and management [29]) have been developed to improve battery performance and safety.

In this paper, large cell voltage deviation in a large-scale grid-tied LTO system at low (∼5%) and high (∼90%) SoC zones and the immediate cut-off mechanism triggered by it are reported. An ECM-based model of a grid-tied battery system is generated and compared with the practical system. The simulation in this study focuses on the impact of the intrinsic CtCV sources found in an LTO battery pack in a limited-time event (a charging and discharging cycle) and the intrinsic CtCV is represented by the difference in ECM component values. Parameter values differ for each cell modelled and are generated at random with a distribution which matches that obtained from multi-cell electrochemical impedance spectroscopy (EIS) sampling. The large-scale battery pack ECM solver that is used in this study for simulation will be presented in detail. The dependency between SoC and the extent of parameters distribution is considered in the model.

2 | CELL VOLTAGE DEVIATION PHENOMENA OBSERVED DURING THE OPERATION OF THE WILLENHALL ENERGY STORAGE SYSTEM

This study uses the Willenhall Energy Storage System (WESS) as an exemplar. WESS is a grid-tied battery research facility with a 2 MW/1 MWh battery pack which consists of 21,120 Toshiba supercharge ion battery (SCiB) LTO cells [30]. The LTO cells inside WESS have an operating voltage window from 1.5 to 2.7 V [31]. A single SCiB LTO cell's diagram and electrical symbol are shown in Figure 1a. Every 24 cells are connected and packed into a 2P12S module which consists of 12 series links of two parallel cells as Figure 1b shows. In WESS the battery pack has 40 parallel racks and each rack is made of 22 series connected 2P12S modules. As a result, the electrical connection in cell level presents a highly symmetrical hierarchical structure as Figure 1c illustrates, where different hierarchical levels are shown in different background colours (pack: red, rack:
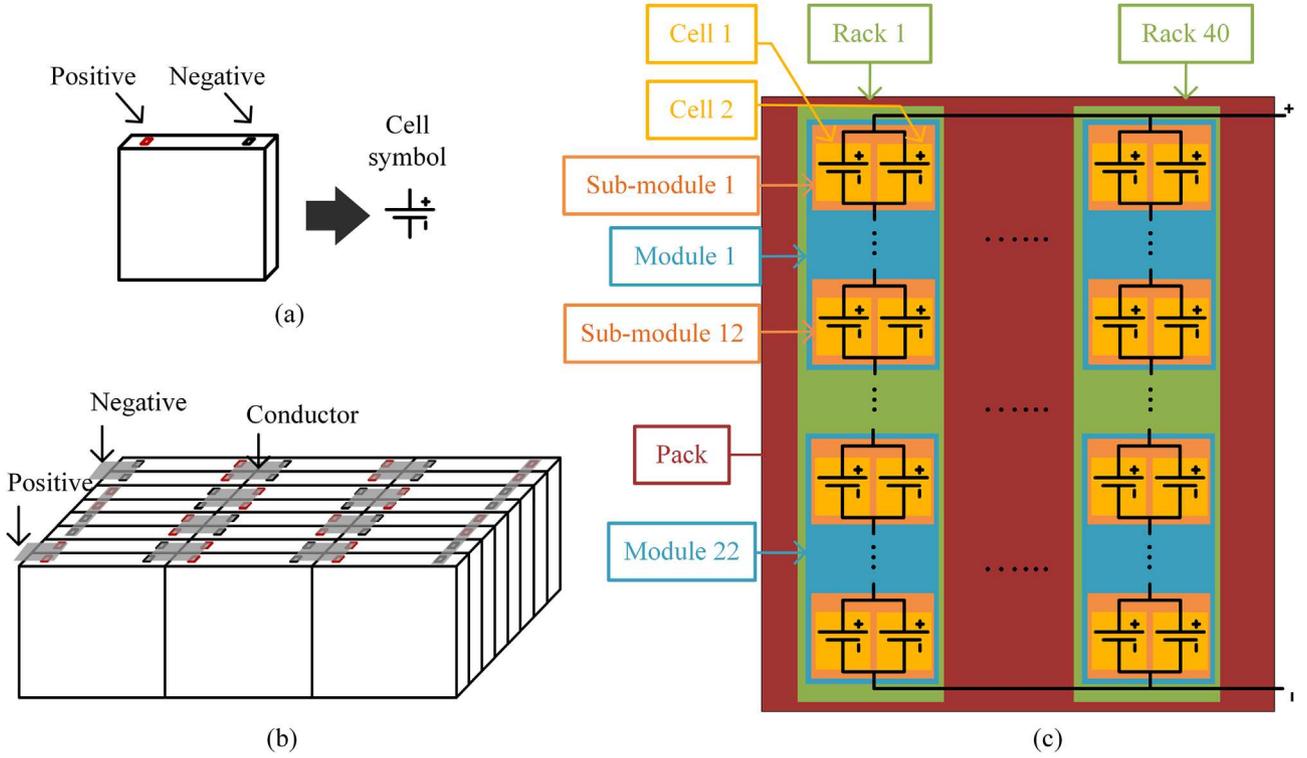
FIGURE 1 Battery connection in WESS: (a) cell diagram and electrical symbol, (b) 2P12S module diagram, (c) pack electrical connection. WESS, Willenhall Energy Storage System

green, module: blue, sub-module: orange, cell: yellow). The sub-module refers to the two parallel cells structure inside the 2P12S module.

Although the structure of the symmetrical electrical connection varies across different applications [32], the overall aim is to guarantee similar currents are applied to all cells to achieve a uniform ageing, SoC and temperature inside the battery. To reduce the manufacturing complicity, a pack is usually constructed using identical modules. However, to achieve same special design purposes, different sizes of modules can be used in a pack. This approach is seen in the Nissan Leaf 2019s battery [33].

2.1 | Maximum allowed cell voltage deviation

During the operation of WESS, some occasional and unexpected cut-off events happen during which the battery is instantly disconnected from the load regardless of the demand. This battery disconnection causes a discontinuity in delivering or absorbing energy and could lead to a penalty in the service it provides (e.g. frequency service). The history data shows that some of these events are caused by voltage deviation in the battery. The BMS in the WESS maintains the voltage deviation at a low level (∼10 mV) through relaxation and passive balancing. In extreme operations, the voltage deviation could exceed the manufacturer's maximum tolerance 150 mV. In this case, the cell imbalance is so severe that the BMS disconnects the bat-

tery in order to protect it. Under these circumstances, it may be necessary to balance the cells manually. Figure 2 shows constant charging even where the charging process is repeatedly interrupted by the BMS due to the maximum voltage deviation restriction. The manufacturer-specified maximum allowed cell voltage deviation is 12.5% of the difference between the LTO cell's higher and lower cut-off voltages.

In this paper, as (1), (2) and (4) define, cell voltage deviation $V_{t,dev}$ refers to the difference (at any given time, t) between $V_{t,max}$ and $V_{t,min}$ which are the maximum and minimum cell terminal voltage in a pack. $V_{t,i}$ is the terminal voltage for cell with identity number i (for WESS i is an integer between 1 and 21,120). [N_R, N_M, N_S, N_C] is used to represent the location of a cell where $N_R \in [1, 40]$, $N_M \in [1, 22]$, $N_S \in [1, 12]$ and $N_C \in [1, 2]$ are the identity of the racks, modules, sub-modules and cells, respectively as Figure 1c shows. The cell identity can be calculated as $i = 528(N_R - 1) + 24(N_M - 1) + 2(N_S - 1) + N_C$. Average cell terminal voltage $V_{t,avg}$ is defined in (3). Similar terms such as cell SoC deviation SoC_{dev} and cell current deviation I_{dev} are defined in the same way.

$$V_{t,max}(t) = \max\left(V_{t,1}(t), V_{t,2}(t), ..., V_{t,\,21120}(t)\right) \quad (1)$$

$$V_{t,min}(t) = \min\left(V_{t,1}(t), V_{t,2}(t), ..., V_{t,\,21120}(t)\right) \quad (2)$$

$$V_{t,avg}(t) = \mathrm{mean}\left(V_{t,1}(t), V_{t,2}(t), ..., V_{t,\,21120}(t)\right) \quad (3)$$
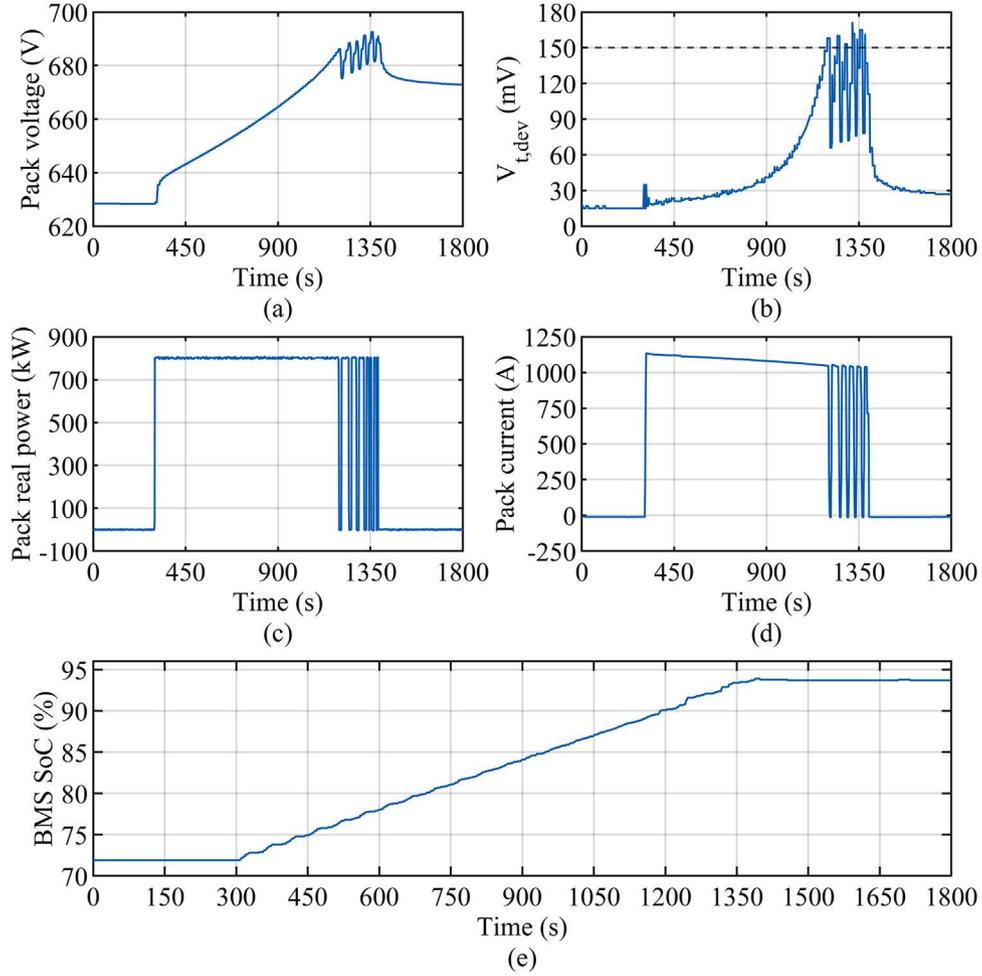
FIGURE 2 Measurements showing BMS cutting of the battery due to the battery exceeding the maximum allowed cell voltage deviation, 150 mV (SoC: from 72.7% to 93.8%): (a) pack voltage, (b) cell voltage deviation, (c) pack power from BMS, (d) pack current and (e) BMS SoC. BMS, battery management system

$$V_{t,dev}(t) = V_{t,max}(t) - V_{t,min}(t) \qquad (4)$$

Figure 2 shows the BMS-recorded performance of WESS during a constant power charge with part (a) showing the pack voltage, (b) the cell voltage deviation, (c) the power provided by the BMS, (d) the pack current and (e) SoC estimated by BMS. It is important to note that the SoC range for a cell in a battery pack is slightly narrower than for that cell alone because the BMS must not over- or under-charge any cell. This means that 0% SoC, reported by the BMS, occurs at a different cell condition to 0% SoC from a single-cell study.

The worst $V_{t,dev}$ scenario in the WESS is in the high SoC zone. When $V_{t,dev}$ reaches the maximum allowed value of 150 mV, as shown Figure 2b, the battery cuts off from the load. After a brief rest, the $V_{t,dev}$ value drops below 150 mV and then the battery is brought back online by the BMS. With the reapplication of the charging current (∼1000 A), the $V_{t,dev}$ is quickly restored to 150 mV in 10–40 s and triggers another cut-off. This process has repeatedly occurred at the end of charge and has caused discontinuities in energy delivery. The first cut-off in Figure 2 happens at around 90% SoC, and the remain-

ing 10% battery capacity cannot be used effectively. Under this circumstance, in frequency service applications, the battery will be unable to absorb extra energy from the grid network even though the battery is not fully charged.

2.2 | Cell voltage deviation in repeated experiments

To explore the changing trend of $V_{t,dev}$ in WESS at the 'full' SoC range, constant load experiments were conducted on the WESS. Figure 3 presents two repeated constant power experiments (855 kW) on WESS. In both experiments, the battery was discharged from 95% SoC to ∼5%; After 1-h resting, the battery was charged to 90% as Figure 3b shows. The battery pack is in a controlled (heated, ventilated and air conditioned) environment which minimises the influence of the ambient environment on the experiments. At the end of discharge, there is a slight SoC difference between two experiments (Exp. 1: 5%, Exp. 2: 7%), as Figure 3b shows. Also, the internal cell-balancing circuit incorporated within the Toshiba battery pack
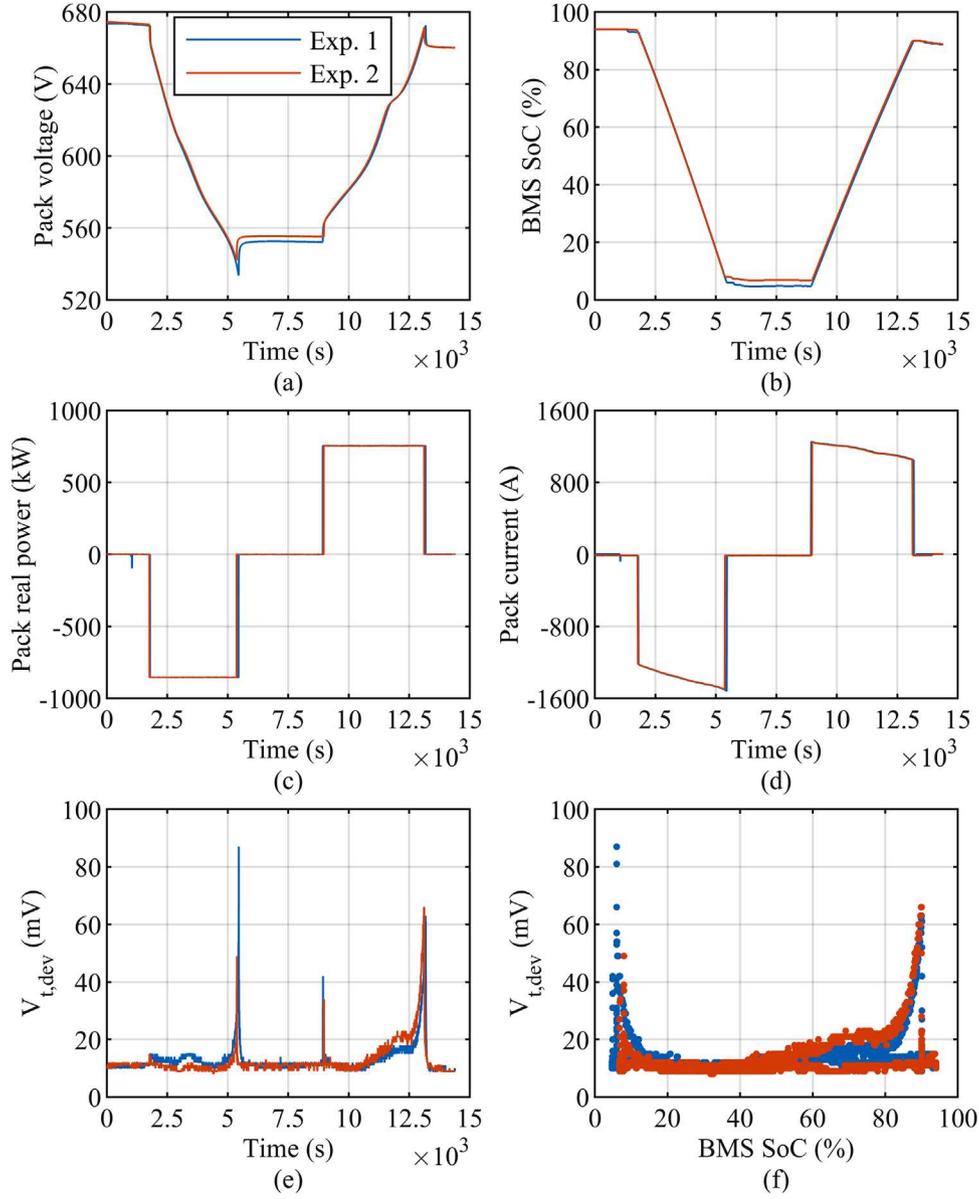
FIGURE 3 Two repeated experiments (blue: experiment 1, red: experiment 2): (a) pack voltage, (b) pack SoC from BMS, (c) pack power from BMS, (d) pack current (charging: positive), (e) cell voltage deviation vs. time, (f) cell voltage deviation vs. BMS SoC. Note: the key for each subfigure is identical

works under the instruction of a propriety BMS which operates outside the user's control.

As Figure 3e and f shows, the two-cell voltage deviation results share similarities in shape and value. At the beginning of both experiments, the battery had the same and stable $V_{t,dev}$ of about 10 mV. The $V_{t,dev}$ had a slight step increase at the beginning of discharge ($\sim$1800 s) and then experienced a long period of fluctuation during further discharge. At the end of discharge ($\sim$5500 s), the deviation value had a rapid increase but ended with different values (exp. 1: 87 mV, exp. 2: 49 mV). Accurately estimating the state of charge is difficult because of non-linearities in the electrochemistry, variability with temperature and recent charge history, and the high level of precision needed for measurement. Inaccurate SoC measurement (leading to imprecise start and stop times) is likely to account for the observed differences.

During the resting processes, $V_{t,dev}$ quickly decays and is restored to 10 mV within a few minutes. At the beginning of charge ($\sim$9000 s), there is a smaller peak of $V_{t,dev}$. After a period of relative stability, $V_{t,dev}$ increases to a large value (exp. 1: 63 mV, exp. 2: 66 mV) at a high charging rate. The similar phenomenon was found in another experiment in WESS and reported in [34]. From the view of the SoC domain, Figure 3f, at the same SoC the $V_{t,dev}$ in the two experiments are close to each other. The peak value of $V_{t,dev}$ appeared at low ($\sim$5%) and high ($\sim$90%) SoC zone.

In contrast to Figure 2, $V_{t,dev}$ does not exceed 150 mV in Figure 3. The main reason is that, during charging, the 150 mV $V_{t,dev}$ happens in high SoC zone (SoC > 90%, as shown in Figure 3). However, to avoid damage caused by a high $V_{t,dev}$, the battery in the experiments shown in Figure 3 was only charged to 90% SoC. The true cell-level SoC is likely lower than 90% because the battery pack voltage is 572 V (compared with 685 V shown in Figure 2a for 90% SoC). The likely cause of the discrepancy is integration error for Couluomb counting by the BMS.

3 | A CELL LEVEL BATTERY PACK EQUIVALENT CIRCUIT MODEL SOLVER

A simulation tool for battery packs is required to study the impact of the cell-voltage deviation phenomenon. ECM is used in this paper where each cell is represented by an equivalent circuit from which the entire battery pack is constructed according to its internal hierarchy. Every cell's ECM parameter information is essential for the battery pack simulator. In the case of the WESS, it is impractical to disassemble the WESS facility and identify the ECM parameter value for each of the 21,120 cells. Instead, all the cells' ECM parameters are assumed as following normal distributions and randomly generated from their mean values and standard deviation which are obtained from preliminary experiments (EIS tests) on four representative cells. The details and partial results of EIS test will be shown in Section 3.3.

In this section, the single-cell ECM and the battery-pack circuit solver (i.e. the simulation tool) will be introduced first. Then the processes related to ECM parameter generation will be explained which mainly consists of three parts: parameter value and distribution identification, generating parameter value and constructing ECM models for individual cells.

3.1 | Single-cell equivalent circuit model

Compared with electrochemical models, ECMs have the advantage of having a lower computational complexity. ECMs also have acceptable performance in emulating cell behaviour (see [22] for an overview of lithium-ion battery modelling methods relevant to SoC estimation). Figure 4a shows a single-cell ECM which consists of an ohmic resistor R_0, parallel-RC branch ($R_1//C_1$) with a time constant related to the cell diffusion process and a voltage source representing the cell equilibrium V_{OC}. The difference between V_{OC} and battery terminal voltage, V_t, is known as the overpotential [35] and noted as V_{over} in this paper. The discretised mathematical model of the cell ECM is given in (5)–(8) where Q is maximum available cell capacity in ampere-seconds and Δt is time step length (1 s). Considering the LTO lifetime and the relationship between capacity retention and coulombic efficiency η [36], η is set as unity for LTO cells in this paper and omitted in the equations. Cell parameters including R_0, R_1, C_1 and V_{OC} are estimated by

their relationship with SoC which are obtained from preliminary experiments.

$$V_t [k] = I [k] \times R_0 [k] + V_{C1} [k] + V_{oc} [k] \quad (5)$$

$$\tau_1 [k] = R_1 [k] \times C_1 [k] \quad (6)$$

$$V_{C1} [k+1] = V_{C1} [k] \times \exp\left(\frac{-\Delta t}{\tau_1 [k]}\right)$$
$$+ R_1 [k] \times I [k] \cdot \left(1 - \exp\left(\frac{-\Delta t}{\tau_1 [k]}\right)\right) \quad (7)$$

$$SoC [k+1] = SoC [k] + \frac{I [k] \times \Delta t}{Q} \quad (8)$$

3.2 | Battery pack equivalent circuit solver

The whole battery pack equivalent circuit can be generated by connecting single cell's equivalent circuits in the electrical structure shown in Figure 1c. If cell current and initial condition are fully known, every cell in a pack can be simulated with (5)–(8). The pack solver was built with the following assumptions: (i) each cell's ECM (such as parameter values and V_{OC}-SoC relationship) and present internal states (such as capacitor voltage, SoC and V_{OC}) are fully known; (ii) during each time step in the solver, the change in ECM parameters value is small and can be considered constant.

Figure 4c illustrates the main processes that occur within the battery pack simulator. The first step in the 'battery pack solver' is to simplify each cell to an equivalent resistor and voltage source as shown in Figure 4b. Then series and parallel connections of cells are combined using Thévenin and Norton theorems. The cell combination process is worked up according to the pack hierarchy from single cell, to sub-module and so on until the pack is finally represented by a single equivalent resistor and voltage source. Subsequently, the internal currents and voltages inside the pack are determined in the sequence of racks, sub-modules and cells through Kirchhoff's current law and Kirchhoff's voltage law. The calculated cell current value is used to update cell SoC and V_{C1} which will be used in next time step. In this way, complicated differential equations for the overall battery-pack equivalent circuit are avoided and the simulation can be conducted efficiently. Elementwise and dimensional matrix operation and graphics processing unit calculation were adopted to boost the simulator's speed.

3.3 | ECM parameter value identification and the extent of ECM parameter variation

ECM parameters used in the battery pack simulator are randomly generated according to the parameter's value and distribution from preliminary experiments on sample cells. To obtain ECM parameters value at different SoC points, EIS tests were
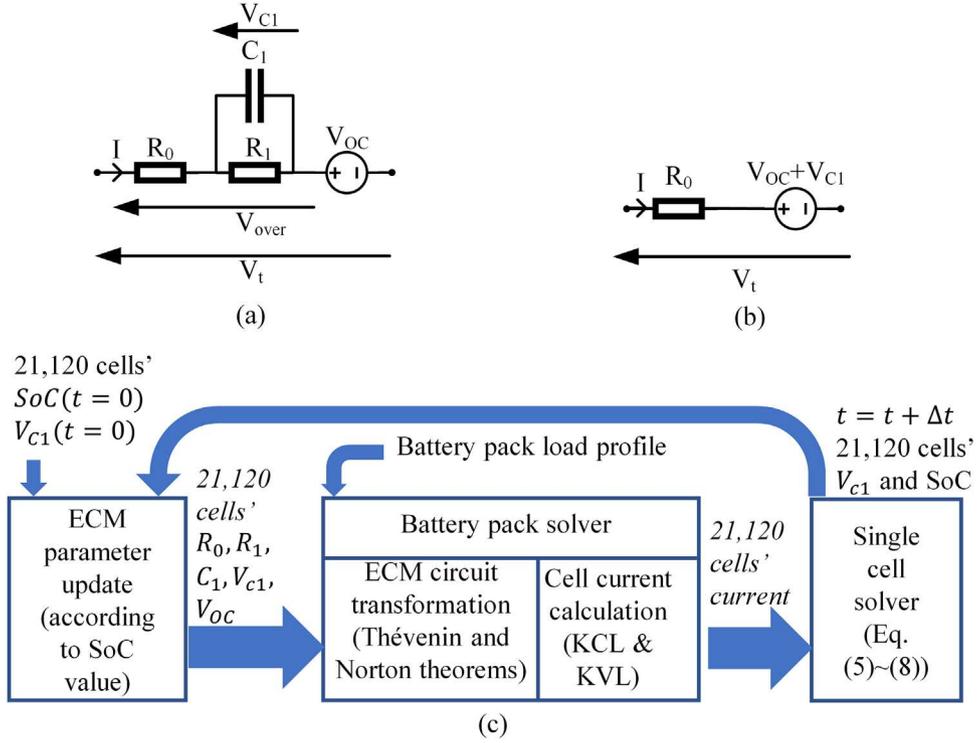
FIGURE 4 Cell ECM and battery pack simulator: (a) one time constant ECM, (b) corresponding Thévenin circuit, (c) battery pack simulation processes. ECM, equivalent circuit models

conducted on four SCiB LTO cells with the same cycle count (400 cycles). The four cells have a slight difference in cycling current: two were cycled with 1 C and two at 2 C rate. However, the cycle counts for different cells are the same. The cycle count is small for LTO cells and not enough to cause significant cell degradation. These cells were labelled from Cell02 to Cell05 and tested at 25°C from 100% to 0 SoC in 10% intervals. In the EIS measurement, the frequency range was set from 5 kHz to 5 mHz.

Only four cells were available for individual measurement. Thus there is reduced confidence in the mean and standard deviations for each cell parameter in WESS. Nevertheless, the existence of the variation, rather than its precise level, is critical for understanding the real-world operation of a BESS.

Figure 5 illustrates the EIS impedance results of the four cells at 50% SoC where Z_{re} and Z_{im} are the real and imaginary parts of the impedance. When Z_{im} is positive, the test results are distorted (Figure 5a). Fortunately, the model in Figure 4a can never have an impedance with a positive imaginary part. Hence, only the EIS result with negative imaginary parts (Figure 5b) was used to identify the parameter's value. An example of ECM fitting results is shown in Figure 5c–f) [37].

The overall fitting results of ECM parameters are presented in Figure 6 (on the left vertical axis). In general, as Figure 6a shows R_0 has a stable value (0.7 mΩ) which slightly decreases as SoC increases. R_1 takes most part of the total resistance R_{total} and dominates the change of it. R_{total} is the total resistance which is equal to sum of R_0 and R_1. Both R_1 and R_{total} have

the highest value at 100% SoC and second-highest value at 0% SoC. Time constant τ_1 in Figure 6b has the highest value at 100% SoC and a peak value at 60% SoC. The results shown in Figure 6 provide ECM parameters of four cells and, more importantly, ECM parameter distribution can be obtained from it.

The previous experiments on WESS in Figure 3 show that $V_{t,dev}$ changes during charging and discharging which indicates that the extent of cell variation in WESS might be different at different SoCs. The coefficient of variation (CoV) is used in this paper to describe the extent of parameter variability through which the relationship between the extent of cell variation and SoC will be explored. For a data set with N elements $A_1, A_2, ..., A_N$, the CoV is defined by the ratio of the standard deviation σ to the mean μ as (9)–(11) show.

$$\sigma = \sqrt{\frac{1}{N-1}\sum_{i=1}^{N}|A_i - \mu|^2} \tag{9}$$

$$\mu = \frac{1}{N}\sum_{i=1}^{N}A_i \tag{10}$$

$$CoV = \frac{\sigma}{\mu} \tag{11}$$

The CoV of different parameters at different SoC is also shown in Figure 6 (in the right vertical axis). Among all the
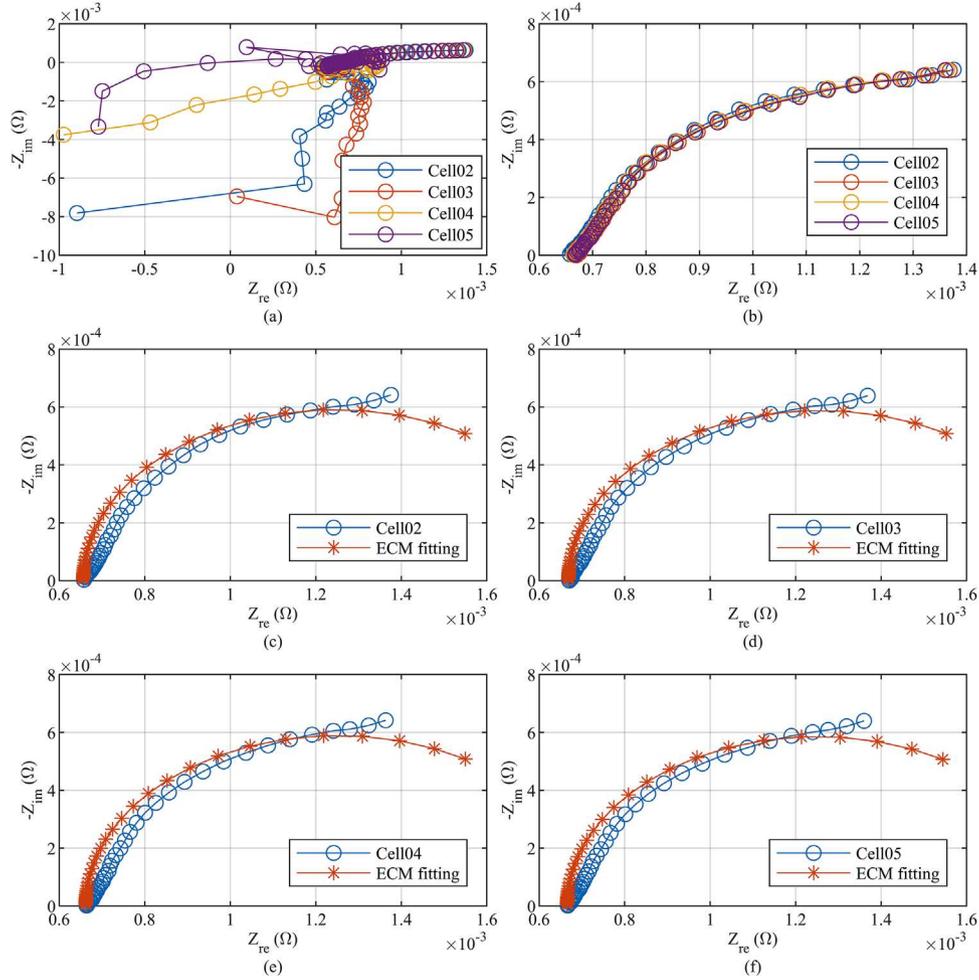
FIGURE 5 EIS and ECM fitting result of 4 LTO cells at 50% SoC: (a) overall result, (b) result when $Z_{im} < 0$, (c)–(f) ECM fitting result from Cell02 to Cell05. EIS, electrochemical impedance spectroscopy

parameters, V_{OC} in Figure 6f has the least CoV around 0.06% (±0.04%) and the largest value of it appears at 100% SoC at 0.1%. As Figure 6a shows, R_0 has a small CoV concentrated at 0.8% (±0.4%). The CoVs of R_1 and C_1 do not have rapid change between 20% and 90% SoC and both have large values at 10% and 100% SoC. R_1 and C_1 are parameters related to the diffusion process. The large CoV indicates more distinct differences in electrical or chemical properties among tested cells, such as the reaction rate. In terms of τ_1, the large CoV only shows up at 100% SoC. The cells capacities were estimated by the Coulomb counting method ($\mu = 20.73$ Ah, $\sigma = 0.03$ Ah).

The cell SoC used in the cell experiments represents a wider operating range than the WESS BMS SoC. As can be observed in the cell SoC experimental data, at the extremes of the SoC curve, $V_{t,dev}$ becomes greater. BESS manufacturers recognise this issue and therefore restrict the operating range of their systems to avoid issues associated with $V_{t,dev}$ at extreme SoC. The parameters' large value of CoV at these SoC regions is believed as an important reason for the high $V_{t,dev}$ observed in Figures 2 and 3.

3.4 | Generating equivalent circuit model parameters value

With the ECM parameters result of EIS tests, ECM parameters used in the battery pack circuit solver can be generated to fit a measured statistical distribution. Before random numbers are generated, the type of distribution must be chosen. Experiment results in the literature reflect that cell parameters reasonably fit normal distributions. In [11], a large number of lithium-ion cells were tested and the results show that cell parameters such as resistance and capacity follow normal distributions to a large extent. The same results are seen in [38, 39]. In the Monte Carlo simulation that follows, all the parameters are assumed to follow normal distributions. The standard deviation σ to the mean μ of each parameter at different SoC was estimated from the EIS results in Figure 6.

ECM parameters among tested cells are not independent of each other. To include the correlation among parameters, in this paper R_0, R_1 and C_1 at every 10% SoC are set as following a joint normal distributed whose probability density function $f(R_0, R_1, C_1)$ is shown in (12). μ_{R0}, μ_{R1} and μ_{C1} are the
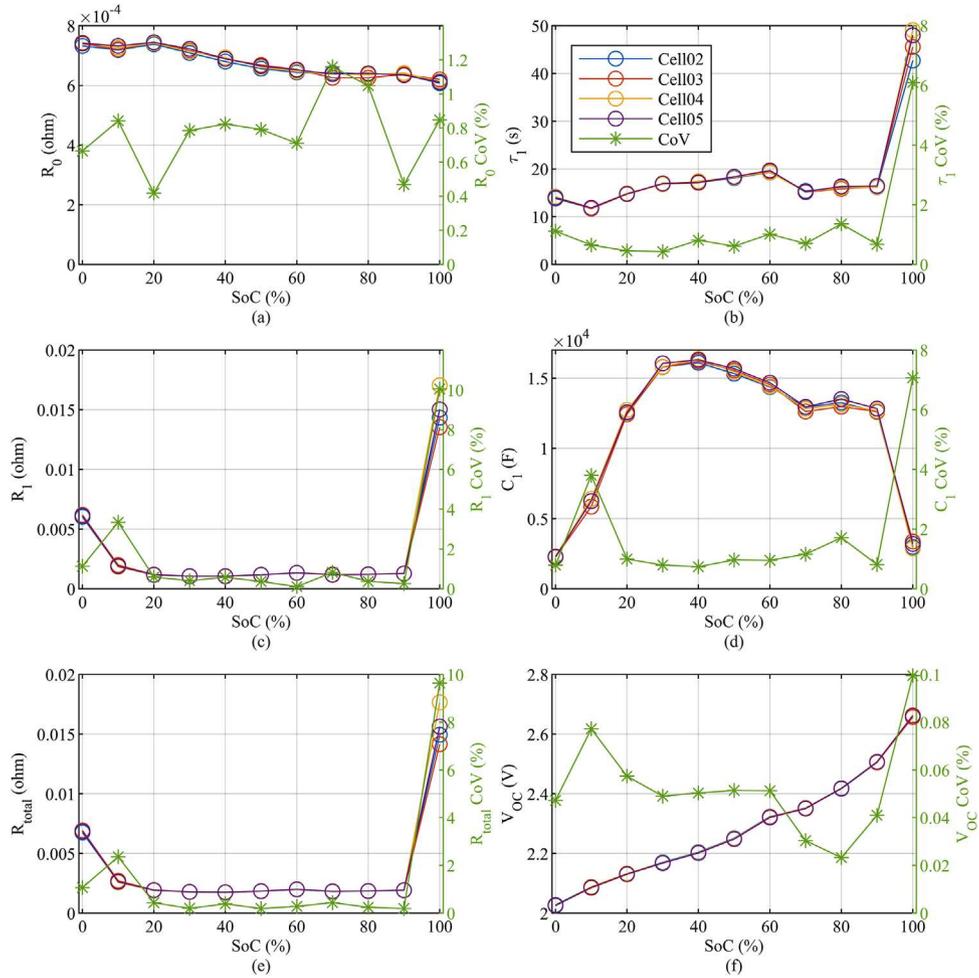
FIGURE 6 Parameter value and the coefficient of variation of: (a) R_0, (b) τ_1, (c) R_1, (d) C_1, (e) R_{total}, (f) V_{OC}. Note: the key for each subfigure is identical

mean of random variables R_0, R_1 and C_1 respectively. Σ is the covariance matrix and shown in (13) where cov(.,.) represents the covariance. From 0% SoC at every 10% SoC, R_0, R_1 and C_1 are generated according to their σ, μ and Σ obtained from cells EIS tests results in Figure 6 and the probability density function in (12).

$$f\ (R_0, R_1, C_1) = \frac{1}{(2\pi)^{\frac{3}{2}} \cdot |\Sigma|^{\frac{1}{2}}} \exp\left(-\frac{1}{2}\left(\begin{bmatrix} R_0 \\ R_1 \\ C_1 \end{bmatrix} - \begin{bmatrix} \mu_{R0} \\ \mu_{R1} \\ \mu_{C1} \end{bmatrix}\right)^T\right.$$
$$\left. \times \Sigma^{-1} \cdot \left(\begin{bmatrix} R_0 \\ R_1 \\ C_1 \end{bmatrix} - \begin{bmatrix} \mu_{R0} \\ \mu_{R1} \\ \mu_{C1} \end{bmatrix}\right)\right) \quad (12)$$

$$\Sigma = \begin{bmatrix} \text{cov}\,(R_0, R_0) & \text{cov}\,(R_0, R_1) & \text{cov}\,(R_0, C_1) \\ \text{cov}\,(R_1, R_0) & \text{cov}\,(R_1, R_1) & \text{cov}\,(R_1, C_1) \\ \text{cov}\,(C_1, R_0) & \text{cov}\,(C_1, R_1) & \text{cov}\,(C_1, C_1) \end{bmatrix} \quad (13)$$

In terms of capacity and V_{OC}, due to the limited sample size from the experiment, it is challenging to identify the most correlated parameters and SoC point to cell capacity Q. As a compromise, Q is set as an independent normal distributed variable in this paper and can be straightforwardly generated for different cells. On the other hand, V_{OC} describes cell equilibrium terminal voltage which is considered irrelevant to the parameters (R_0, R_1 and C_1) who are related to cell dynamic properties. Therefore, V_{OC} is set as an independent variable as well. Besides, as mentioned in Section 3.1, the coulombic efficiency for all cells is set as 100% so that the effect of coulombic efficiency variation among cells is not included in this paper. To ensure the resulting cell templates are physically realisable the random number generator used by the Monte Carlo analysis has a lower bound of zero.

3.5 | Constructing models for individual cells

Building the model of R_0, R_1 and C_1 is the most complex part of constructing ECMs for individual cells which are divided into three steps. Step 1: the values of R_0, R_1 and C_1 at different SoC
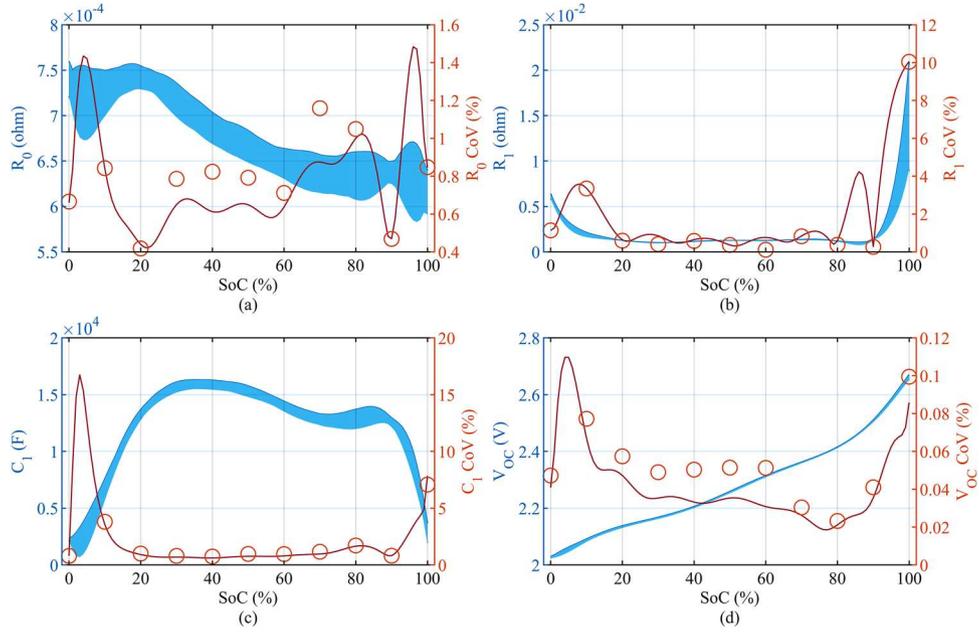
FIGURE 7 A randomly generated WESS-sized battery, all cells' ECM parameters and their CoVs (red inline: CoV of generated pack; circle points: CoV from EIS experiment): (a) R_0, (b) R_1, (c) C_1, (d) V_{OC} vs. SoC

(0, 10%, …, 100%) for all 21,120 cells are randomly generated as Section 3.4 describes. Step 2: the randomly generated parameter in step 1 is regrouped according to their cell identity. Step 3: the parameter and SoC relationship is modelled using polynomial equations cell by cell. A diagram demonstrating this process is provided in Figure A.1. The method of generating V_{OC}-SoC model for each cell is similar.

An example of a generated battery is illustrated in Figure 7 in which the cyan areas contain all 21,120 cells' parameter-SoC relationship. In another word, for a cell in the generated pack, its parameter-SoC relationship is located inside the cyan regions. The red line in Figure 7 represents the parameter CoV of all 21,120 cells in the generated pack and the red circles are parameter CoV from the previous cells EIS experiment shown in Figure 6. In general, the parameters value and CoV in the generated pack are consistent with the experiment results in Figure 6. So far, the essential preparation for battery pack simulation has been done which includes building a battery pack simulator and generating random battery packs.

4 | MONTE CARLO SIMULATION: CONSTANT POWER LOAD

Monte Carlo simulation is a commonly used method to study the impact of ECM parameter variation on battery packs and has been used, for example in [12] and [40]. In Monte Carlo simulations, many ECM parameter sets are generated. Each parameter value is chosen at random according to the probability density function for that parameter. Thus a large number of simulations, all with different but realistic parameters, are performed. These simulations show the sensitivity

of the model to random variation which a single simulation cannot do.

In this section, 100 randomly generated WESS-sized battery packs are simulated under a constant power load (855 kW). The simulation results provide a general changing trend of variables such as battery voltage, current and $V_{t,dev}$, under the specified load and predetermined parameter uncertainty. In each simulation, all the 21,120 cells are set as 95% SoC which is consistent with the initial battery SoC value in the experiments shown in Figure 3 . The cells are connected into a pack according to the electrical connection in Figure 1c. Because of the variation in cell V_{OC}–SoC relationship, cells have slightly different terminal voltages. This terminal voltage difference is decreased by a 10-min rest through self-balancing during which the terminal voltage difference among cells causes an internal cell current through the internal electrical connection in the pack. After resting, the maximum cell self-balancing current decreases to a small value (0.005 C-rate). A small (or zero) self-balancing current indicates that the battery pack cannot be further effectively balanced by itself. Then, the pack is discharged at constant power until it meets cut-off requirements.

After another 10-min rest, the battery is charged until cut-off. In this simulation, to avoid over-charging and over-discharging the cells, the battery pack is cut off when any cell voltage reaches cut-off voltages or any cell SoC is outside the range of 0% to 100% or the $V_{t,dev}$ exceeds 150 mV.

In this simulation, some parameters in the model are bounded in certain ranges. The SoC is defined as the ratio of available cell capacity to the maximum cell capacity which is a value non-negative number and is smaller than 100%, therefore, is bounded by 0% $\leq$ SoC $\leq$ 100%. According to the datasheet for Toshiba LTO cell, the cell voltage should be
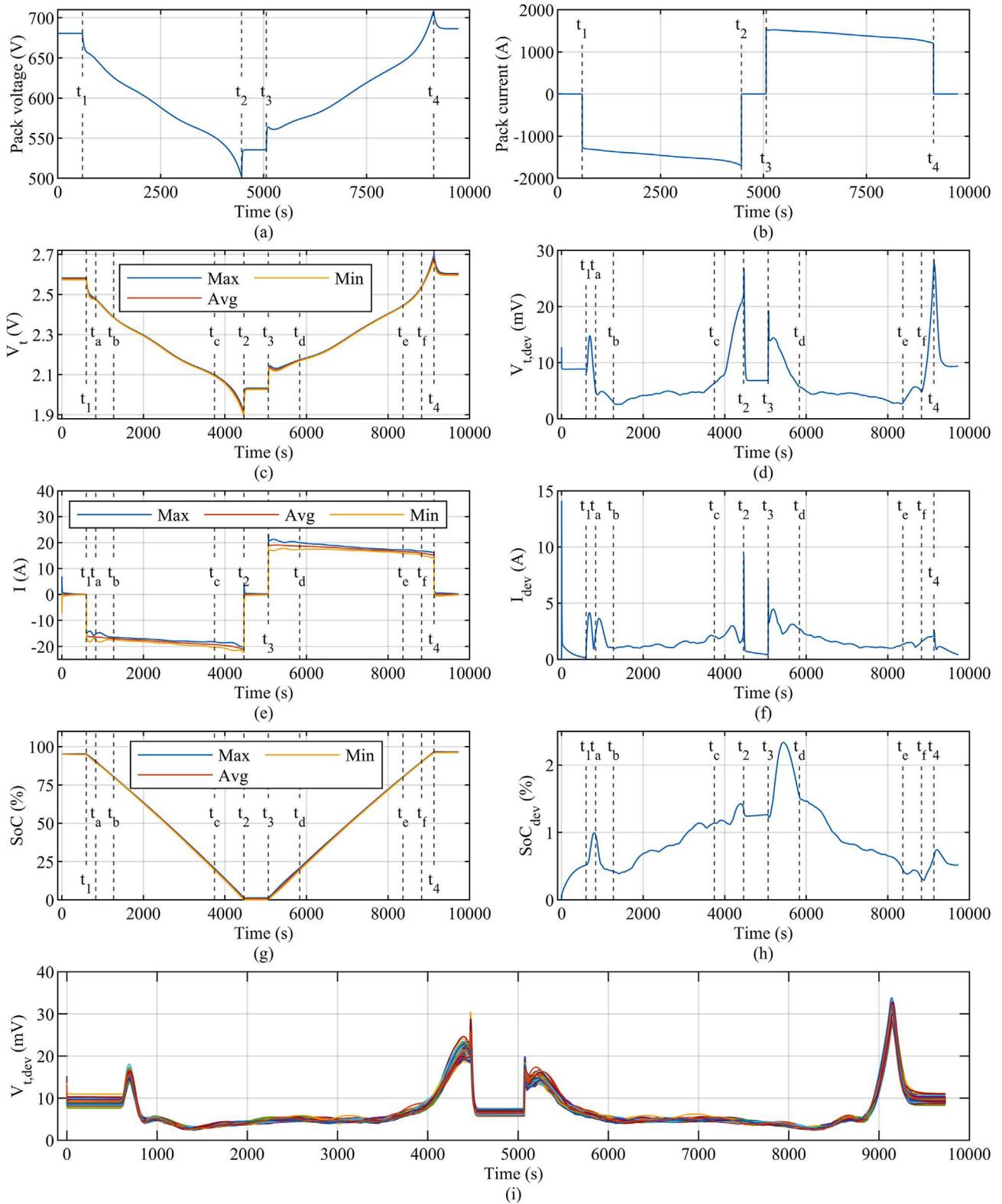
FIGURE 8 Overall Monte Carlo simulation result and the result from a single simulation. (a) Battery pack voltage, (b) pack current, (c, d) cell terminal voltage and deviation, (e, f) cell terminal current and deviation, and (g, h) cell SoC and deviation in the single simulation. t_1: 600 s (t_2: 4465 s, t_3: 5060 s, t_4: 9130 s; t_a: 832 s, t_b: 1271 s, t_c: 3744 s, t_d: 5832 s, t_e: 8369 s, t_f: 8826 s). (i) Cell terminal voltage deviation of 100 times Monte Carlo simulation

FIGURE 9 Terminal voltages at the end of discharge for 21,120 cells in the pack (result from a single simulation, from t_c: 3744 s to t_2: 4465 s)
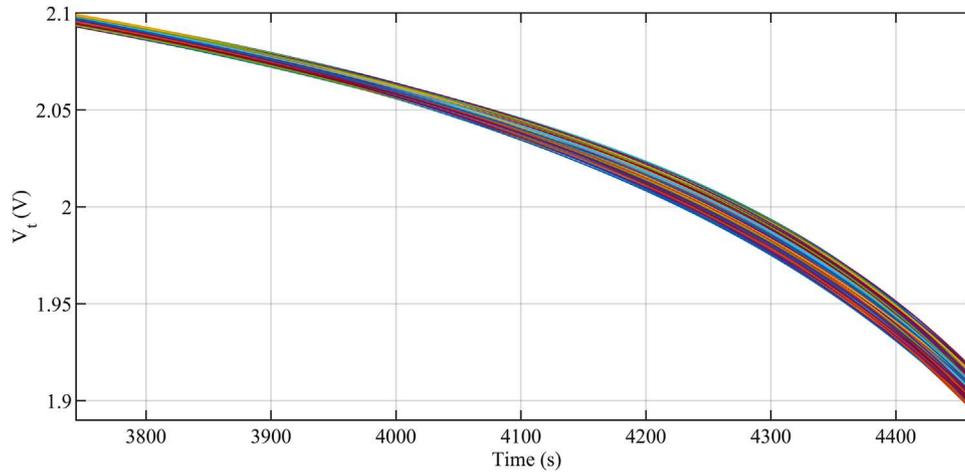
controlled between 1.5 and 2.7 V. As a result, the cell terminal voltage is bounded by $1.5\,\text{V} \leq V_t \leq 2.7\,\text{V}$. The BMS of WESS does not allow a cell voltage deviation $V_{t,dev}$ exceeding 150 mV. Besides, $V_{t,dev}$ is defined as the instantaneous difference between the maximum cell voltage and the minimum cell voltage of the whole pack. Consequently, the cell terminal voltage is bounded by $0 \leq V_{t,dev} \leq 150$ mV. According to this load power profile, the battery-pack current (the input of the ECM) is calculated by the battery-pack equivalent circuit solver and used for simulation. Compared with the experiments in Figure 3, the simulation explored a wider SoC range and conducted a shorter rest period.

4.1 | Results from a single simulation: at the pack and cell level

The Monte Carlo simulation provides 100 similar simulation results with slightly different timelines. For example, because of CtCV, battery packs have different parameters (e.g. capacity, internal resistance) so that batteries were cut off at different times in different simulations. To clearly describe the simulation process, one of the Monte Carlo simulations using the parameter set in Figure 7 is chosen to be discussed first.

Figure 8a and b shows the pack level simulation result of the chosen simulation. Time instants from t_1 to t_4 in the figure represent the start or end of the discharging or charging. It is interesting to note that in a constant load simulation, the magnitude of battery current, as shown in Figure 8b, is increasing during the discharging process and decreasing during charging because of the decreasing and increasing battery voltage, respectively. This current change is also observed during the constant load experiment in Figure 3.

The cell level simulation results of the single simulation are shown in Figure 8c–h. Apart from t_1 to t_4, six more time instants, t_a to t_f, are labelled in the figure at which cell average SoC reaches some critical values (t_a and t_f: 90%, t_b and t_e: 80%, t_c and t_d: 20%). The most important finding in the single constant power simulation result is the relationship between the ECM

parameter variation and the cell deviations that a large parameter variation causes a large deviation in the pack. Between SoC zones of 0%–20% and 90%–100%, all cell ECM parameters have a large CoV, as Figure 7 shows. Correspondingly, during t_1 to t_a, t_c to t_2, t_3 to t_d and t_f to t_4 when the battery pack is being discharged or charged in these two SoC zones, the battery pack is more unbalanced and shows a large value of $V_{t,dev}$, and I_{dev}.

It is worth mentioning the result during t_a to t_b and t_e to t_f when the cells are in the 80%–90% SoC range. According to Figure 7, in this SoC range, R_1 which dominates the total internal resistance also has a large CoV. However, $V_{t,dev}$ is small during t_a to t_b and t_e to t_f for two possible reasons. First, between 80% and 90% SoC, the other parameters such as V_{OC} and C_1 have a smaller CoV compared with 0%–20% and 90%–100% SoC as Figure 7. Second, the value of R_1 is small between 80% and 90% SoC which is unable to induce a large V_{over} and voltage difference. Consequently, a small $V_{t,dev}$ is witnessed in this SoC zone.

Inside a large-scale battery pack, the cell voltage is not only influenced by the cell properties (such as the impedance and capacity) but also the cell connection topology, cell current distribution, load current, initial cell SoC etc. During the simulation, the particular cells which have the maximum and minimum terminal voltages vary as different cells lose or gain voltage at different rates. There is not a single dominant cell which is maximum or minimum for a long time. The terminal voltages of all 21,120 cells at the end of discharge (t_c to t_2) in the single simulation are plotted in Figure 9 where each line represents the voltage change of an individual cell and thus the shaded area is the total cell voltage range. The results show that there is no single cell which is clearly an outlier.

4.2 | Results from all Monte Carlo simulation

To obtain an overall view of the cell deviation inside WESS sized pack with the given parameter distribution under constant power load, 100 Monte Carlo simulations were conducted, and the results are presented in Figure 8i. There are 100 lines in

Figure 8i and each of them represents the $V_{\text{t,dev}}$ result from one of the 100 Monte Carlo simulations. As Figure 8i shows, all simulations have a similar changing trend in terminal voltage and current deviations but with slightly different values. The finding in the previous single-simulation example is still valid in the Monte Carlo simulation result that a large $V_{\text{t,dev}}$ shows up at the beginning and end of charging and discharging where the cells have a large ECM parameter CoV and large internal resistance.

The $V_{\text{t,dev}}$ results in simulations share similarities with that in WESS experiments (Figure 3). In terms of the changing trend, both simulation and experiment witnessed a high $V_{\text{t,dev}}$ at high and low SoC zone and also relatively small $V_{\text{t,dev}}$ in between. However, in WESS experiments the $V_{\text{t,dev}}$ in the beginning of discharging is not as obvious as that in simulation for unknown reasons. In terms of value, $V_{\text{t,dev}}$ in simulation is smaller than exp. 1 and exp. 2 in Figure 3. The cell balancing circuit in WESS and the error in ECM parameters' CoV are the possible reasons for it.

5 | CONCLUSION

This study raises the awareness of the maximum allowed $V_{\text{t,dev}}$ and the impact of SoC on cell variance which help the design of a BESS and the cell balancing technique. As found in the paper, the BMS may have an intense reaction when the $V_{\text{t,dev}}$ exceeds the threshold value. For example, the battery is cut off in WESS. In most cases, the settings in a BMS cannot be changed by operators. The cut-off reaction benefits the safety of the battery but may not be acceptable in a smart grid that requires consistent energy delivery.

It is challenging to reproduce the $V_{\text{t,dev}}$ in a real facility through simulation due to the system nonlinearities and ambient environment complexity. This study used an ECM to represent every cell in a battery pack and the simulation shows the similarity with the $V_{\text{t,dev}}$ trends observed in experiments. However, the 150 mV $V_{\text{t,dev}}$, observed experimentally, was not observed during simulations. Nevertheless, the demonstration of the cause of the trends and their distributions is meaningful for studying and understanding large-scale BESSs.

Some multi-cell batteries contain balancing circuits to keep the cell voltage or SoC deviation under control. Normally, the balancing circuit is triggered when the $V_{\text{t,dev}}$ value reaches a setting value regardless of the SoC value. However, the simulations for WESS LTO battery packs in this paper show that it is more likely that a high $V_{\text{t,dev}}$ will occur at the extremes of SoC. This is one reason why manufacturers de-rate the SoC operating envelope. Battery packs featuring internal balancing mechanisms would alleviate some of these issues. Concepts such as Brillpower's intelligent battery management technology could extend the operating envelope thereby reduce the levelised cost of energy.

NOMENCLATURE

$A_1, A_2, \ldots A_N$	elements of a data set
C_1	the capacitor in $R_1//C_1$ branch
I_{dev}	cell current deviation
R_0	ohmic resistor
R_1	the resistor in $R_1//C_1$ branch
R_{total}	the total resistance ($R_{total} = R_0 + R_1$)
SoC_{dev}	cell SoC deviation
V_{C1}	voltage crossing $R_1//C_1$ branch
V_{OC}	open-circuit voltage
V_{over}	cell overpotential
$V_{\text{t,avg}}$	average cell voltage in a pack
$V_{\text{t,dev}}$	cell terminal voltage deviation
$V_{\text{t,max}}$	maximum cell voltage in a pack
$V_{\text{t,min}}$	minimum cell voltage in a pack
V_{t}	cell terminal voltage
Z_{im}	the imaginary part of cell electroimpedance
Z_{re}	the real part of cell electroimpedance
$t_1, \ldots, t_4, t_a, \ldots, t_f$	time instants in a simulation
$\mu_{\text{R0}}, \mu_{\text{R1}}$ and μ_{C1}	the mean value of R_0, R_1 and C_1
τ_1	time constant caused by $R_1//C_1$ branch
$\text{cov}(.,.)$	covariance of two variables
I	current
N	elements number
N_{C}	the identity of the cells
N_{M}	the identity of the modules
N_{R}	the identity of the racks
N_{S}	the identity of the sub-modules
Q	capacity
$f(R_0, R_1, C_1)$	joint probability density function of R_0, R_1 and C_1
t	time
Δt	time step length
Σ	covariance matrix
η	coulombic efficiency
μ	mean value
σ	standard deviation

CONFLICT OF INTEREST
The authors have no known competing financial interests or personal relationships that could have appeared to influence the work reported in this paper.

DATA AVAILABILITY STATEMENT
This work has not generated its own data, beyond that shown in the paper.

ORCID
Zeyuan Wang https://orcid.org/0000-0001-9050-1826
Jonathan Davidson https://orcid.org/0000-0002-6576-3995

REFERENCES
1. Harris, K., Michaels, C., Rose, S., Gower, A., Martin, V., Spry, W.: Energy Trends: UK electricity (2021). https://www.gov.uk/government/statistics/energy-trends-section-6-renewables
2. Yildirim, B., Elgendy, M., Smith, A., Pickert, V.: Evaluation and comparison of battery cell balancing methods. In: 2019 IEEE PES Innov.

Smart Grid Technol. Eur., pp. 1–5 (2019). https://doi.org/10.1109/ISGTEurope.2019.8905588

3. Duarte, R., Moreira, L., Barros, L.A.M., Monteiro, V., Afonso, J.L., Pinto, J.G.: Power converters for a small islanded microgrid based on a micro wind turbine and an battery energy storage system. In: ECOS 2018 Proceedings of the 31st International Conference on Effic. Cost, Optim. Simul. Environ. Impact Energy Syst., Guimarães, Portugal, pp. 1–12 (2018)

4. Lu, L., Han, X., Li, J., Hua, J., Ouyang, M.: A review on the key issues for lithium-ion battery management in electric vehicles. J. Power Sources. 226, 272–288 (2013). https://doi.org/10.1016/j.jpowsour.2012.10.060

5. Gong, X., Xiong, R., Mi, C.C.: Study of the characteristics of battery packs in electric vehicles with parallel-connected lithium-ion battery cells. In: Conference Proceedings IEEE Appl. Power Electron. Conf. Expo. APEC, pp. 3218–3224 (2014). https://doi.org/10.1109/APEC.2014.6803766

6. Dubarry, M., Vuillaume, N., Liaw, B.Y.: Origins and accommodation of cell variations in Li-ion battery pack modeling. Int. J. Energy Res. 34, 216–231 (2010). https://doi.org/10.1002/er.1668

7. Farahani, G.: DC–DC series-resonant converter with multi-stage current-driven for balance charger of series-connected lithium-ion batteries. IET Power Electron. 14, 992–1007 (2021). https://doi.org/10.1049/pel2.12081

8. Zhou, L., Zheng, Y., Ouyang, M., Lu, L.: A study on parameter variation effects on battery packs for electric vehicles. J. Power Sources. 364, 242–252 (2017). https://doi.org/10.1016/j.jpowsour.2017.08.033

9. Zilberman, I., Ludwig, S., Jossen, A.: Cell-to-cell variation of calendar aging and reversible self-discharge in 18650 nickel-rich, silicon–graphite lithium-ion cells. J. Energy Storage. 26, 100900 (2019). https://doi.org/10.1016/j.est.2019.100900

10. Barreras, J.V., Raj, T, Howey, D.A., Schaltz, E.: Results of screening over 200 pristine lithium-ion cells. In: 2017 IEEE Veh. Power Propuls. Conference, pp. 1–6 (2018). https://doi.org/10.1109/vppc.2017.8331060

11. Rumpf, K., Naumann, M., Jossen, A.: Experimental investigation of parametric cell-to-cell variation and correlation based on 1100 commercial lithium-ion cells. J. Energy Storage. 14, 224–243 (2017). https://doi.org/10.1016/j.est.2017.09.010

12. An, F., Chen, L., Huang, J., Zhang, J., Li, P.: Rate dependence of cell-to-cell variations of lithium-ion cells. Sci. Rep. 6, 1–7 (2016). https://doi.org/10.1038/srep35051

13. Zilberman, I., Schmitt, J., Ludwig, S., Naumann, M., Jossen, A.: Simulation of voltage imbalance in large lithium-ion battery packs influenced by cell-to-cell variations and balancing systems. J. Energy Storage. 32, 101828 (2020). https://doi.org/10.1016/j.est.2020.101828

14. Kenney, B., Darcovich, K., MacNeil, D.D., Davidson, I.J.: Modelling the impact of variations in electrode manufacturing on lithium-ion battery modules. J. Power Sources. 213, 391–401 (2012). https://doi.org/10.1016/j.jpowsour.2012.03.065

15. Shin, D., Poncino, M., Macii, E., Chang, N.: A statistical model-based cell-to-cell variability management of Li-ion battery pack. IEEE Trans. Comput. Des. Integr. Circuits Syst. 34, 252–265 (2015). https://doi.org/10.1109/TCAD.2014.2384506

16. Wu, Y., Keil, P., Schuster, S.F., Jossen, A.: Impact of temperature and discharge rate on the aging of a $LiCoO_2$/$LiNi_{0.8}Co_{0.15}Al_{0.05}O_2$ lithium-ion pouch cell. J. Electrochem. Soc. 164, A1438–A1445 (2017). https://doi.org/10.1149/2.0401707jes

17. Stroe, A.I., Stroe, D.L., Knap, V., Swierczynski, M., Teodorescu, R.: Accelerated lifetime testing of high power lithium titanate oxide batteries. In: 2018 IEEE Energy Convers. Congr. Expo. ECCE 2018, pp. 3857–3863. (2018). https://doi.org/10.1109/ECCE.2018.8557416

18. Cao, X., Zhao, N.: A cooperative management strategy for battery energy storage system providing enhanced frequency response. Energy Rep. 8, 120–128 (2022). https://doi.org/10.1016/j.egyr.2021.11.092

19. Alnuman, H., Gladwin, D.T., Foster, M.P.: Novel control method for improving energy efficiency of DC electric railways. In: IEEE International Conference Control Autom. ICCA, pp. 91–96. IEEE Computer Society (2019). https://doi.org/10.1109/ICCA.2019.8899576

20. Qin, Q., Guo, T., Lin, F., Yang, Z.: Energy transfer strategy for urban rail transit battery energy storage system to reduce peak power of trac-

tion substation. IEEE Trans. Veh. Technol. 68, 11714–11724 (2019). https://doi.org/10.1109/TVT.2019.2948766

21. Park, S., Ahn, J., Kang, T., Park, S., Kim, Y., Cho, I., Kim, J.: Review of state-of-the-art battery state estimation technologies for battery management systems of stationary energy storage systems. J. Power Electron. 20, 1526–1540 (2020). https://doi.org/10.1007/s43236-020-00122-7

22. Meng, J., Luo, G., Ricco, M., Swierczynski, M., Stroe, D.-I., Teodorescu, R.: Overview of lithium-ion battery modeling methods for state-of-charge estimation in electrical vehicles. Appl. Sci. 8, 659 (2018). https://doi.org/10.3390/app8050659

23. Song, Z., Yang, X.-G., Yang, N., Delgado, F.P., Hofmann, H., Sun, J.: A study of cell-to-cell variation of capacity in parallel-connected lithium-ion battery cells. ETransportation 7, 100091 (2021). https://doi.org/10.1016/j.etran.2020.100091

24. Ziegler, A., Oeser, D., Hein, T., Montesinos-Miracle, D., Ackva, A.: Reducing cell to cell variation of lithium-ion battery packs during operation. IEEE Access 9, 24994–25001 (2021). https://doi.org/10.1109/ACCESS.2021.3057125

25. Hosseinzadeh, E., Arias, S., Krishna, M., Worwood, D., Barai, A., Widanalage, D., Marco, J.: Quantifying cell-to-cell variations of a parallel battery module for different pack configurations. Appl. Energy. 282, 115859 (2021). https://doi.org/10.1016/j.apenergy.2020.115859

26. WAGMAN, D.: Dispute Erupts Over What Sparked an Explosive Li-ion Energy Storage Accident - IEEE Spectrum (2020). https://spectrum.ieee.org/dispute-erupts-over-what-sparked-an-explosive-liion-energy-storage-accident (accessed 23 February 2022)

27. Hill, D.: McMicken battery energy storage system event technical analysis and recommendations (2020). https://www.aps.com/-/media/APS/APSCOM-PDFs/About/Our-Company/Newsroom/McMickenFinal TechnicalReport.ashx?la=en&hash=50335FB5098D9858BFD276C40FA 54FCE (accessed 23 February 2022)

28. Rehman, M.M.U., Evzelman, M., Hathaway, K., Zane, R., Plett, G.L., Smith, K., Wood, E., Maksimovic, D.: Modular approach for continuous cell-level balancing to improve performance of large battery packs. In: 2014 IEEE Energy Convers. Congress Expo., pp. 4327–4334 (2014). https://doi.org/10.1109/ECCE.2014.6953991

29. Lamb, J., Jeevarajan, J.A.: New developments in battery safety for large-scale systems. MRS Bull. 46, 395–401 (2021). https://doi.org/10.1557/s43577-021-00098-0

30. Rogers, D., Gladwin, D., Stone, D., Strickland, D., Foster, M.: Willenhall Energy Storage System: Europe's largest research-led lithium titanate battery. Eng. Technol. Ref. 4, 1–6 (2017). https://doi.org/10.1049/etr.2016.0121

31. Industrial Lithium-ion Battery SCiB™ Industrial Pack series | TOSHIBA Rechargeable battery SCiB™, (n.d.). https://www.scib.jp/en/product/sip/index.htm#sipspec (accessed 9 December 2020)

32. Zwicker, M.F.R., Moghadam, M., Zhang, W., Nielsen, C.V.: Automotive battery pack manufacturing – a review of battery to tab joining. J. Adv. Join. Process. 1, 100017 (2020). https://doi.org/10.1016/j.jajp.2020.100017

33. Electric vehicle lithium-ion battery | NISSAN | TECHNOLOGICAL DEVELOPMENT ACTIVITIES (n.d.). https://www.nissan-global.com/EN/TECHNOLOGY/OVERVIEW/li_ion_ev.html (accessed 14 January 2021)

34. Fantham, T.L., Gladwin, D.T.: Impact of cell balance on grid scale battery energy storage systems. In: Energy Reports, pp. 209–216. Elsevier Ltd, Amsterdam (2020). https://doi.org/10.1016/j.egyr.2020.03.026

35. Ovejas, V.J., Cuadras, A.: State of charge dependency of the overvoltage generated in commercial Li-ion cells. J. Power Sources. 418, 176–185 (2019). https://doi.org/10.1016/j.jpowsour.2019.02.046

36. Xiao, J., Li, Q., Bi, Y., Cai, M., Dunn, B., Glossmann, T., Liu, J., Osaka, T., Sugiura, R., Wu, B., Yang, J., Zhang, J.G., Whittingham, M.S.: Understanding and applying coulombic efficiency in lithium metal batteries. Nat. Energy. 5, 561–568 (2020). https://doi.org/10.1038/s41560-020-0648-z

37. Jean-Luc, D.: Zfit - File Exchange - MATLAB Central (2021). https://uk.mathworks.com/matlabcentral/fileexchange/19460-zfit (accessed 28 January 2021)

38. Brand, M.J., Hofmann, M.H., Steinhardt, M., Schuster, S.F., Jossen, A.: Current distribution within parallel-connected battery cells. J. Power Sources. 334, 202–212 (2016). https://doi.org/10.1016/j.jpowsour.2016.10.010

39. Paul, S., Diegelmann, C., Kabza, H., Tillmetz, W.: Analysis of ageing inhomogeneities in lithium-ion battery systems. J. Power Sources. 239, 642–650 (2013). https://doi.org/10.1016/j.jpowsour.2013.01.068

40. Chang, F., Roemer, F., Baumann, M., Lienkamp, M.: Modelling and evaluation of battery packs with different numbers of paralleled cells. World Electr. Veh. J. 9, 8 (2018). https://doi.org/10.3390/wevj9010008

APPENDIX A: THE PROCESS OF GENERATING R_0, R_1 AND C_1 MODEL IN ECM FOR EACH CELL

The figure in this appendix demonstrates the process of constructing ECMs for 21,120 cells using R_0, R_1 and C_1 as an example. The process is divided into three steps including generating random numbers, reorganising the generated numbers, and constructing parameter models.
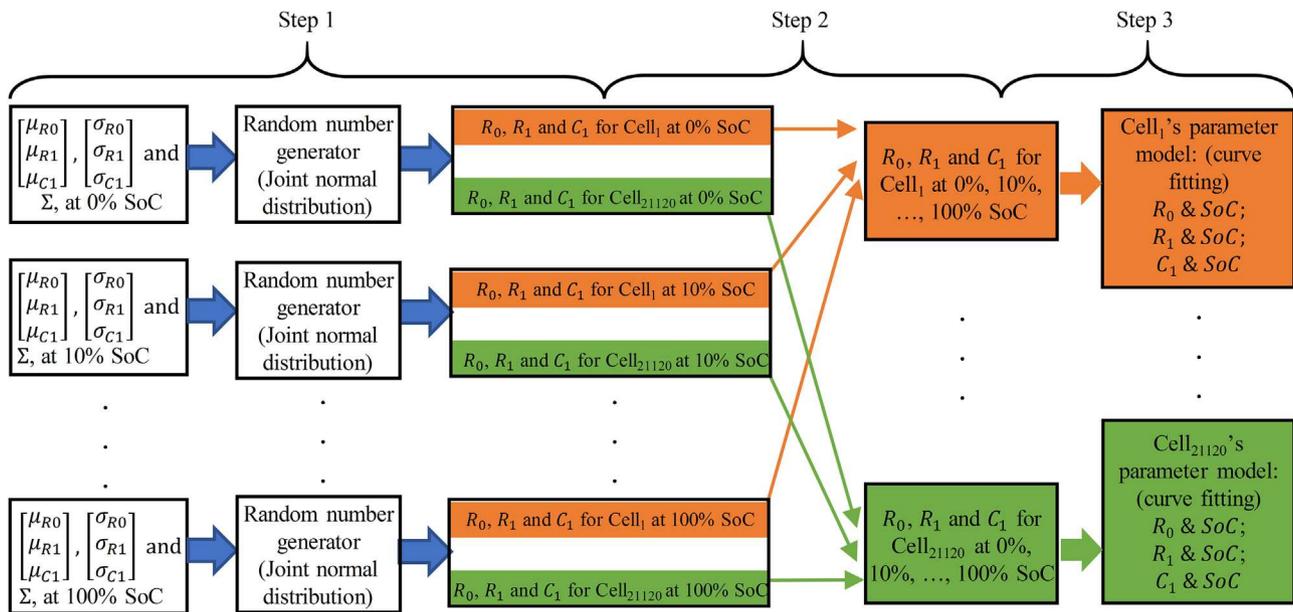

FIGURE A1 The process of generating and modelling R_0, R_1 and C_1 at full SoC range for 21,120 number of cells. Step 1: random value generating for different cells at different SoC points. Step 2: reorganise the random value, gather parameter value for the same cell at different SoC into the same group. Step 3: obtain parameter–SoC relationship for each cell by curve fitting